ACS OMEGA

Article

http://pubs.acs.org/journal/acsodf

Special Magnetic Catalyst with Lignin-Reduced Au−Pd Nanoalloy

Guocheng Han,[†,§] Xiaoyun Li,[†,‡,§] Jiaming Li,[†] Xiaoying Wang,*[,†,‡] Yu Shrike Zhang,*[,‡] and Runcang Sun[†]

[†]State Key Laboratory of Pulp and Paper Engineering, South China University of Technology, Guangzhou 510640, China

[‡]Division of Biomedical Engineering, Department of Medicine, Brigham and Women's Hospital, Harvard Medical School, Boston 02139, United States

Supporting Information

ABSTRACT: This study describes a new strategy to fabricate a special magnetic catalyst via facile coating Au−Pd nanoalloy catalysts onto a commercial magnetic stirring bar, without the incorporation of iron element. First, the abundant natural "waste" lignin was utilized as the reducing and stabilizing agent to prepare Au−Pd nanoalloys in a green manner. The Au−Pd nanoalloys were assumed to have a core−shell structure with an Au-rich core and a Pd-rich shell. The Au−Pd nanoalloys could be well dispersed in aqueous medium due to the stabilizing effect of lignin and be conveniently coated onto the surface of a commercial stirring bar. The $Au_{1.0}Pd_{1.0}$ nanoalloy catalyst exhibited excellent catalytic activities in the reduction of 4-nitrophenol to 4-amnophenol by $NaBH_4$, with a rate constant (k) of 0.239 min^{-1}, which was higher than that of $Au_{0.5}Pd_{1.0}$ and $Au_{2.0}Pd_{1.0}$ nanoalloys and 4 times higher than that of a single-component Au or Pd nanoparticles. Besides, the catalytic ability of Au−Pd nanoalloy catalyst could be maintained even after seven cycles of catalysis. The catalytic rate constant was found to be positively correlated to the stirring speed of the bar. The scanning electron microscopy analysis revealed ravines and pores on the surface of lignin−nanoalloys composites, implying the possible mechanism of the catalytic activities. This study not only proved the feasibility of lignin for green synthesis of Au−Pd nanoalloys but also proposed a facile and innovated strategy for the future production of solid/liquid catalytic platforms where the developed method could be used to coat any surface interfacing the reagents.

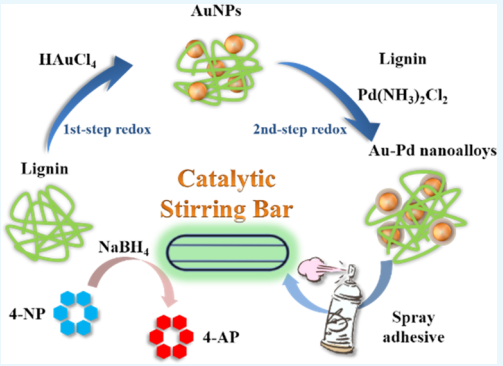

INTRODUCTION

For catalysts, efficient recovery is one of the most important and challenging characteristics, leading to an explosion of interest in those that are easily recoverable. Supported catalysts and magnetic catalysts are the two main solutions for such a purpose. For example, efforts have been made to immobilize the catalysts onto films, ceramics, or carbons,[1−3] but they generally involve complicated fabrication procedures; magnetic components have been incorporated directly into the catalysts,[4,5] but the recovery of magnetic catalysts typically in the powder form is still time-consuming. Therefore, a breakthrough in the fabrication strategy for facile and easily recoverable catalysts is in great demand.

Furthermore, heterogeneous catalysts based on metal nanoparticles (NPs) have played a fundamental role for decades due to their remarkable activities toward various essential reactions.[6] Moreover, alloying two metals into single particles, that is, manufacturing of nanoalloys is now pushing forward the development of catalysis because nanoalloy catalysts usually exhibit enhanced catalytic performance, selectivity, and stability due to the synergistic effects.[7]

Among various techniques for the preparation of nanoalloys, toxic reducing agents as well as additional stabilizers (such as polymers or surfactants) are often needed.[8] More recent with green chemistry, certain natural products such as leaf extracts and fruit juice were employed for the green synthesis of nanoalloys.[9,10] However, these products require intentional extraction for large-scale usage. To avoid unnecessary extraction and the accompanied cost, it would be a better choice to adopt a more abundant natural "waste" as the green reducing and stabilizing agent. Lignin, the second most abundant natural polymer, which is the massive byproduct of the paper industry, turned out to be an ideal candidate for a low-cost and green synthesis of size-controlled and well-dispersed monometallic nanoparticles.[11]

In the present study, we further identified the feasibility of lignin for the synthesis of bimetallic nanoparticles, that is, Au−Pd nanoalloys. The lignin-reduced Au−Pd nanoalloys were facilely coated on a commercial magnetic stirring bar via a spray adhesive to generate a novel heterogeneous catalytic platform. A common reaction involving the reduction of 4-nitrophenol (4-NP) to 4-amnophenol (4-AP) by $NaBH_4$ was demonstrated as a model catalytic reaction. The procedure is illustrated in Scheme 1. The effect of Au−Pd ratio and the stirring speed on

Received: June 20, 2017
Accepted: August 10, 2017
Published: August 24, 2017

DOI: 10.1021/acsomega.7b00830
ACS Omega 2017, 2, 4938−4945

Scheme 1. Illustration of the Synthesis of Core−Shell Au−Pd Nanoalloy with Lignin as the Reducing and Stabilizing Agent and the Fabrication Process of the Au−Pd Nanoalloy-Coated Catalytic Stirring Bar for 4-NP Reduction

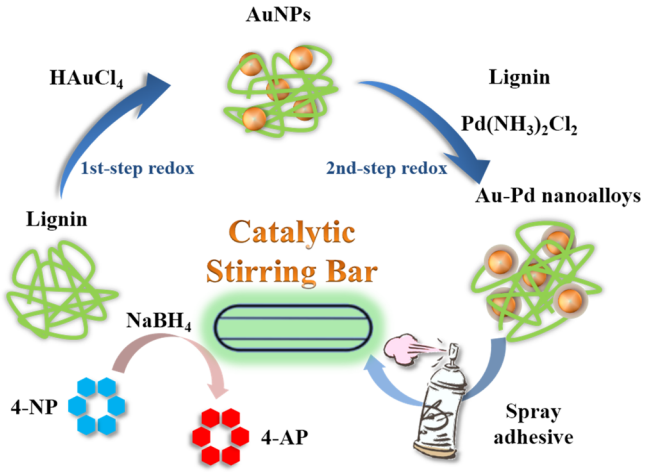

the catalytic performance, as well as the reusability of the catalytic stirring bar, were investigated. We finally propose a possible working mechanism of the Au−Pd nanoalloy-coated catalytic stirring bar.

RESULTS AND DISCUSSION

Structure of Au−Pd Nanoalloys. The compositions of the prepared nanoalloys were examined with the atomic absorption spectrometer (AAS) and the results are shown in Table 1. It can be seen that the Au/Pd ratios of the metal precursors and the final products were similar, indicating that the reaction degrees of the two reduction processes were also similar.

Table 1. Compositions of Different Au−Pd Nanoalloys

precursor	final products		
samples	Au (mmol)	Pd (mmol)	Au:Pd
$Au_{2.0}Pd_{1.0}$	1.07	0.69	1.55:1
$Au_{1.0}Pd_{1.0}$	0.84	0.97	0.87:1
$Au_{0.5}Pd_{1.0}$	0.52	1.06	0.49:1
Au NPs	1.33	0	100:0
Pd NPs	0	1.58	0:100

The UV−vis spectra of the Au−Pd nanoalloys and the single-component Au NPs as well as Pd NPs are shown in Figure 1a. In the first step, the reddish solution of the Au NPs reduced by lignin showed a characteristic absorption band at approximately 530 nm, which could be ascribed to the surface plasmon resonance (SPR) of the Au NPs.[12] In accord with the previous study,[13] the Pd NPs did not show pronounced SPR bands in the UV−vis region. For the three kinds of Au−Pd nanoalloys, it could be observed that the absorbance of the Au NPs SPR band was weakened. In addition, with a higher percentage of Pd, the SPR band became less visible. Therefore, the decrease in the SPR band intensity provided an evidence for the formation of the nanoalloys.[14,15]

XRD can help distinguish the structure of Au−Pd NPs because the diffraction peaks can predict the relationship between the crystal lattice parameter.[16] The XRD patterns of the Au−Pd nanoalloys are shown in Figure 1b, with the patterns of the single-constituent Au NPs and Pd NPs as controls. For Au NPs, there were five reflection peaks at 2θ = 38.2, 44.4, 64.6, 77.6, and 81.7°, corresponding to the (111), (200), (220), (311), and (222) facets, respectively. The pattern of Pd NPs showed four reflection peaks at 2θ = 39.6, 45.5, 67.3, and 80.0°, corresponding to the (111), (200), (220), and (311) facets, respectively. For the alloy structure, the Au and Pd atoms are mixed, and the diffraction peak for the (111) plane should appear between 38.2 and 39.6°.[17] In our fabricated Au−Pd NPs, the (111) diffraction peaks were all located at 2θ = 38.2°, matching that of the Au NPs, and the same with the (200), (220) , and (311) planes. These data indicate that the Au−Pd NPs might have assumed a core−shell structure, with Au atoms in the core and a Pd-enriched shell, which is in accordance with the previous reports.[18]

XPS has been used to determine the surface elemental compositions of the samples. Figure 1c,d illustrates the Pd 3d and Au 4f XPS spectra of the Au−Pd nanoalloys. The binding energies (BEs) of the XPS spectra were calibrated with reference to C 1s at 284.80 eV. In Figure 1c, it can be observed that Pd $3d_{5/2}$ and Pd $3d_{3/2}$ signals appeared at the binding energies (BEs) of 335.80 and 340.90 eV, respectively, suggesting the presence of metallic Pd^0 in each sample.[17] With the increasing Pd percentage, the intensity of Pd signals became stronger. It is worth noting that the two peaks at 338.00 and 343.30 eV corresponding to Pd^{II} were also present in the nanoalloys samples, indicating the increasing positively charged Pd in the nanoalloys, which might be attributed to Au acting as an electronic promoter for Pd.[18,19] Figure 1d illustrates the Au 4f XPS spectra of the nanoalloys samples, presenting the peaks at ∼83.60 and ∼87.30 eV, respectively, which could be assigned to Au $4f_{7/2}$ and Au $4f_{5/2}$ spin−orbit states of the zero-valent Au.[20] The Au^0 4f peaks showed a slight shift but similar BEs when Pd was incorporated into the nanoalloy.

The structural change of lignin during the redox process is illustrated by the Fourier transform infrared (FT-IR) spectra in Figure S1. The spectra of lignin before (spectrum a) and after the reaction (spectra b−d) were similar. The band at 3320 cm^{-1} ascribed to O−H stretching of lignin after the reaction (spectra b−d) was weakened and shifted to lower wavenumbers (3190 cm^{-1}), indicating the decrease in hydroxyl groups within lignin and an interaction between the two metallic counterparts. In spectrum a, there is a 1706 cm^{-1} band belonging to the unconjugated C═O stretching of ester in raw lignin, whereas the 1603 cm^{-1} band was the aromatic skeletal vibration related to the C═O stretching.[21] After the reaction, the unconjugated C═O units of ester were oxidized by metal salt and transformed to carboxylate ion (COO^-), resulting in the disappearance of the 1706 and 1603 cm^{-1} bands, and the occurrence of the 1580 cm^{-1} band.[22] It is noted that in the spectra b−d, there was diminishing of the band at 1220 cm^{-1} corresponding to the phenolic hydroxyl stretching of lignin, implying that some units of the lignin framework reacted or dropped out during the formation of the nanoalloys.[23] In summary, the reduction in the intensity of O−H and the oxidation of the unconjugated C═O to COO^- implied that O−H and C═O units within the lignin structure may have contributed to the reduction of metal salt to nanoalloys.

Morphology of Au−Pd Nanoalloys. Transmission electron microscopy (TEM) and high-resolution TEM (HRTEM) are particularly useful to obtain information of the morphology as well as the angstrom level of the nanoalloys.[24] Figure 2a demonstrates the morphology of $Au_{1.0}Pd_{1.0}$ nano-

DOI: 10.1021/acsomega.7b00830
ACS Omega 2017, 2, 4938−4945

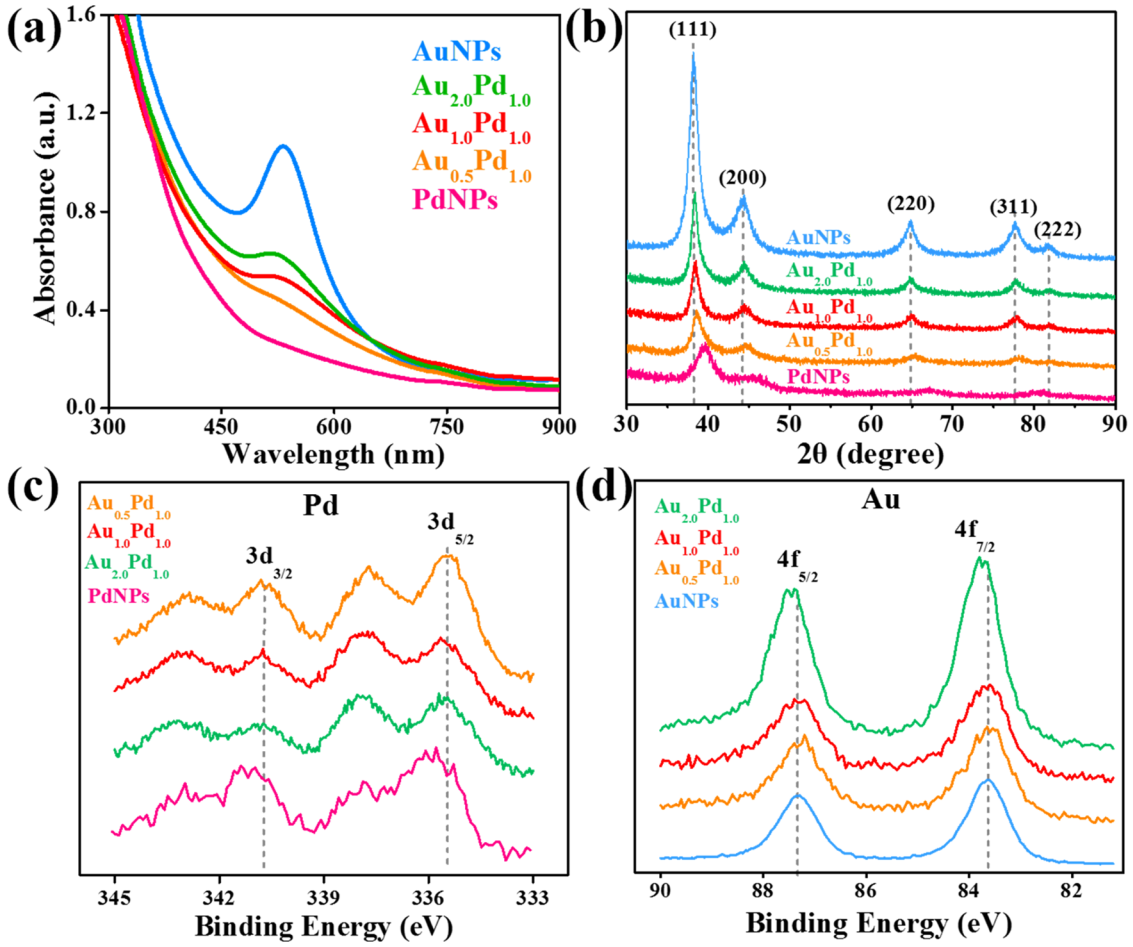

Figure 1. (a) UV−vis spectra of Au−Pd nanoalloys, with the band at 530 nm indicating the formation of Au NPs and the decreasing intensity indicating the nanoalloy formation. (b) X-ray diffraction (XRD) patterns of Au−Pd nanoalloys. The (111) reflection peak shifts from Au to Pd indicates the formation of the nanoalloy. (c) High-resolution Pd 3d X-ray photoelectron spectroscopy (XPS) spectra of the nanoalloys and (d) high-resolution Au 4f XPS spectra of the nanoalloys. The two peaks (at 338.00 and 343.30 eV) corresponding to Pd^{II} in the nanoalloy indicates the positively charged Pd with Au as the electronic promoter.

alloys, which were well dispersed in water due to the stabilization effect of lignin. The size of the nanoalloys ranged from 20 to 50 nm, and the irregular shapes of the nanoalloys might be caused by the utilization of amorphous biopolymer as the reducing agent and an uncritical synthesis condition. In the HRTEM image of Au−Pd NPs (Figure 2b), the dark interiors were the Au-rich cores and the lighter entities on the peripheries were Pd-rich shells. The clear contrast between the Au cores and the Pd shells indicated the core−shell structure of the Au−Pd NPs, which is in accordance with the literature.[24] In addition, the overlay of Pd and Au energy-dispersive spectrometry (EDS) maps (Figure 2c−e) verified the core−shell structure with Au cores embraced by Pd shells.

Catalytic Activity of Stirring Bar-Supported Au−Pd Nanoalloy Catalyst. 4-NP is a common organic pollutant in waste water, and its removal is an important issue. In addition, 4-AP is a potent intermediate for the manufacture of many analgesic/antipyretic drugs and photographic developers. Therefore, ways that efficiently reduce 4-NP to 4-AP have great impact on both environment and industry.[25] In this study, the reduction of 4-NP to 4-AP by $NaBH_4$ was used as a model system to quantitatively evaluate the catalytic activity of the fabricated Au−Pd nanoalloys catalytic magnetic stirring bars. Figure 3a shows a characteristic absorption band of 4-NP at ∼400 nm in the UV−vis spectra, which is proportional to the concentration of 4-NP during the catalytic reaction.[26] It can be seen that the band of 4-NP around 400 nm gradually diminished along with the reaction time and a new band at ∼300 nm ascribed to 4-AP gradually rose, indicating the reduction of 4-NP to 4-AP by $NaBH_4$ in the presence of the catalytic stirring bar. Comparing Pd NPs and Au NPs with nanoalloys (Figures 3a−c and S2), $Au_{1.0}Pd_{1.0}$ nanoalloys presented the best catalytic activity. After being catalyzed by $Au_{1.0}Pd_{1.0}$ nanoalloys for 16 min, 4-NP was almost entirely converted into 4-AP, as shown in Figure 3a. The relationships between the rate constant and the time can be calculated by eq 1[27]

$$\frac{dC_t}{dt} = \ln\left(\frac{C_t}{C_0}\right) = \ln\left(\frac{A_t}{A_0}\right) = -kt \quad (1)$$

This formula indicates that the rate constant (k) is determined by the linear relationship between the reaction time and $\ln(C_t/C_0)$, which is proportional to the $\ln(A_t/A_0)$. In eq 1, C_t represents the concentration of 4-NP at time t and C_0 is the original concentration of 4-NP; A_t refers to the absorbance value at 400 nm at time t and A_0 is the absorbance value at t = 0.

DOI: 10.1021/acsomega.7b00830
ACS Omega 2017, 2, 4938−4945

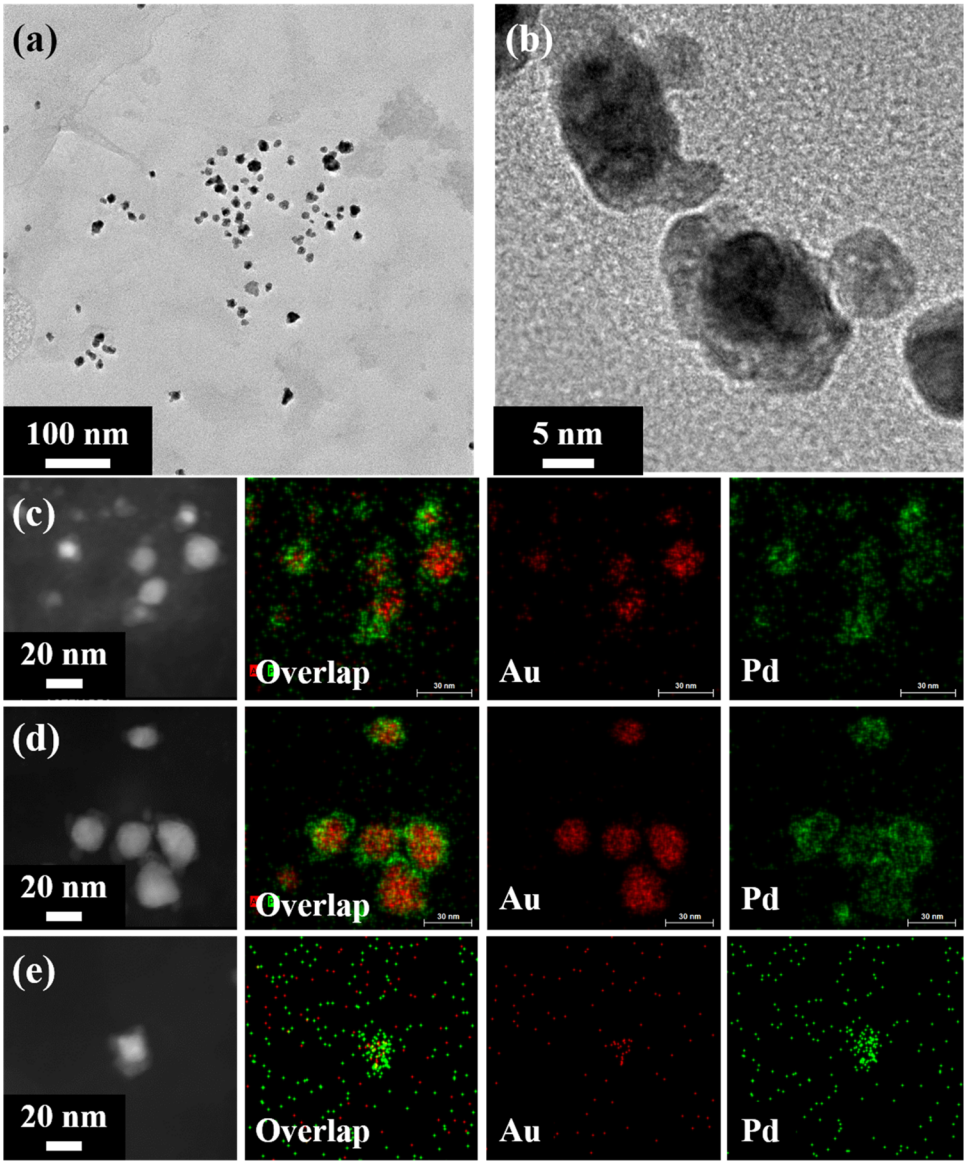

Figure 2. (a, b) TEM images of $Au_{1.0}Pd_{1.0}$ nanoalloys. Scanning transmission electron microscopy (STEM) images and the corresponding EDS mappings of (c) $Au_{0.5}Pd_{1.0}$, (d) $Au_{1.0}Pd_{1.0}$, and (e) $Au_{2.0}Pd_{1.0}$. Most of the Au−Pd nanoalloys had a core−shell segregated structure.

Thus, the rate constant (k) of the five catalysts were calculated to be $Au_{1.0}Pd_{1.0}$ = 0.239 min^{-1}, $Au_{0.5}Pd_{1.0}$ = 0.119 min^{-1}, $Au_{2.0}Pd_{1.0}$ = 0.092 min^{-1}, Pd NPs = 0.072 min^{-1}, and Au NPs = 0.068 min^{-1}. The corresponding data are also illustrated in Figure 3d. These results implied that the Au−Pd core−shell nanoalloys possessed enhanced catalytic efficiency relative to their monometallic counterparts in such a catalytic reaction, which is in agreement with the previous studies.[28,29] Concerning the similar size distribution of the three Au−Pd NPs (Figure S3), $Au_{1.0}Pd_{1.0}$ performed better than $Au_{0.5}Pd_{1.0}$ and $Au_{2.0}Pd_{1.0}$, which might be attributed to a better "synergistic effect" when the molar ratios of the two components are similar.[30]

Additionally, the effect of stirring speed on the catalytic activity was also studied, and the results are shown in Figure 3e. When the catalytic stirring bar was static in the mixed solution of 4-NP and $NaBH_4$, the reduction reaction proceeded slowly, with a low rate constant (k) of approximately 0.013 min^{-1}. With increasing stirring speed, the catalytic stirring bar exhibited enhanced catalytic activities, which could be ascribed to an improved "mass transfer" due to more frequent contact of the reactants and the Au−Pd nanoalloys on the surface of the stirring bar under higher stirring speeds.[31]

The feasibility and reusability are two important properties for a good catalyst. The reusability of our developed catalytic stirring bar was thus also evaluated. As shown in Figure 3f, the Au−Pd nanoalloys catalysts exhibited similar catalytic performance without an obvious decrease in the rate constant (k) over seven consecutive experiments, which might be attributed to the stabilization effect of the lignin matrix on the nanoalloys and the protection of the spray adhesive. After reaction, the stirring bar coated with Au−Pd nanoalloys catalyst could be easily recycled from the reaction vessel and cleaned with water for the next cycle.

The fabricated Au−Pd nanoalloys-coated catalytic stirring bar showed a nearly black gross appearance, which was the natural color of the lignin-synthesized Au−Pd nanoalloys (inset in Figure 4a1). To further investigate the surface texture of the fabricated catalytic stirring bar and the structural changes after catalysis, the SEM images were taken, as shown in Figure 4.

DOI: 10.1021/acsomega.7b00830
ACS Omega 2017, 2, 4938−4945

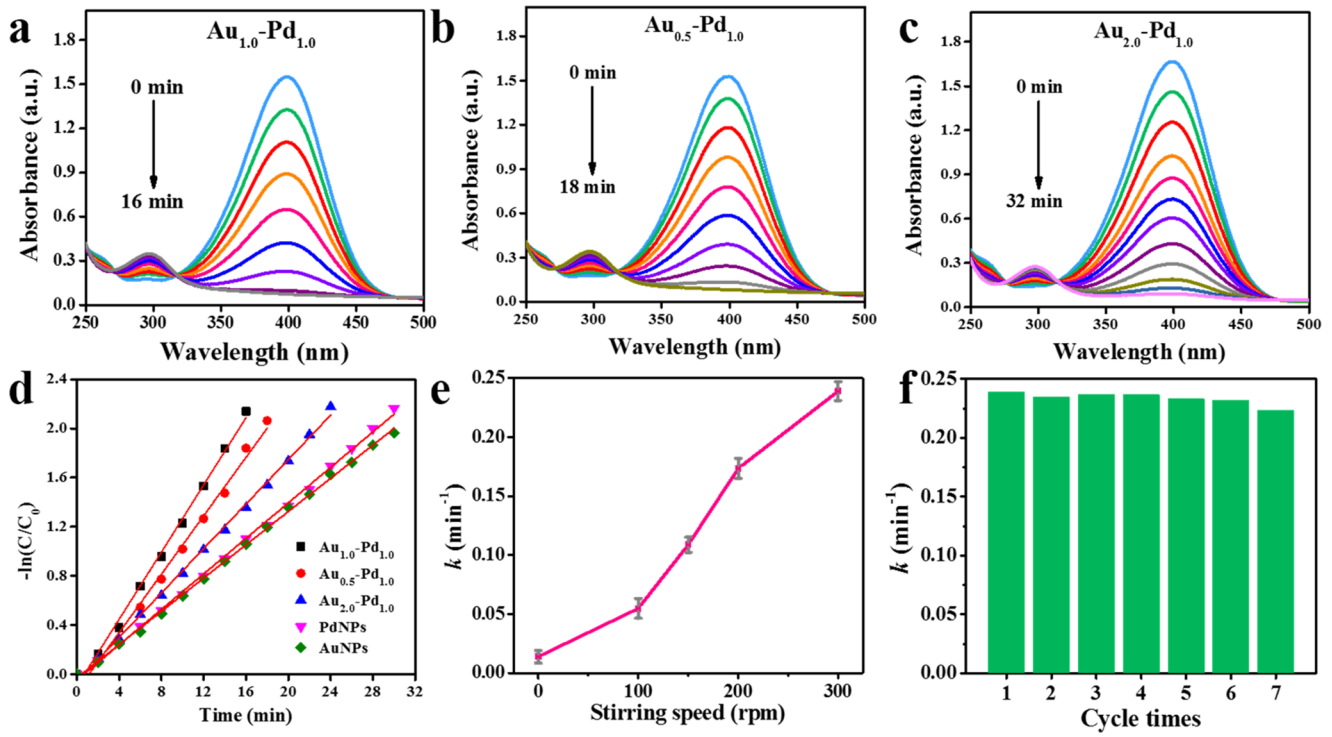

Figure 3. Time-dependent UV−vis spectra showing the reduction of 4-NP by $NaBH_4$ in the presence of (a) $Au_{1.0}Pd_{1.0}$, (b) $Au_{0.5}Pd_{1.0}$, and (c) $Au_{2.0}Pd_{1.0}$ nanoalloys-coated catalytic stirring bar. (d) Plot of $-\ln(C_t/C_0)$ against the reaction time. $Au_{1.0}Pd_{1.0}$ nanoalloys showed the best catalytic activity due to shortest catalytic time. The rate constant of $Au_{1.0}Pd_{1.0}$ was 0.239 min^{-1}. (e) The influence of stirring speed on the rate constant. (f) The reusability performance of $Au_{1.0}Pd_{1.0}$ nanoalloys-coated catalytic stirring bar. The Au−Pd nanoalloy catalyst still exhibited excellent reusability after seven cycles.

From Figure 4a1, it can be seen that the surface of the stirring bar is rough and covered potentially by the mixture of spray adhesive and lignin−nanoalloys composites. The surface was filled with microscopic ravines and pores due to vigorous stirring during the fabrication process. After several cycles of catalysis, the microscopic surface became less rough (Figure 4a2,a3, which might be explained by the external swollen lignin). In spite of this observation, the ravines and pores still remained within the structure, maintaining a large specific surface area for mass diffusion and transport and therefore high efficiency of the heterogeneous catalysis.[32] From the higher-magnification images at nanoscale in Figure 4b, the surface of lignin−nanoalloys layer before catalysis was relatively smooth, with small nodules expected to be the Au−Pd nanoalloys (seen in Figure 4b1). After catalysis for several cycles, the surface became rougher, exposing more internal Au−Pd nanoalloys (Figure 4b2,b3).

Based on the above analyses, the mechanism for Au−Pd nanoalloys-coated catalytic stirring bar to catalyze the reduction of 4-NP to 4-AP by $NaBH_4$ can be explained by the Langmuir−Hinshelwood model,[33] which is illustrated in Scheme 2. Under magnetic stirring, the substrates 4-NP and the reducing agents BH_4^- diffused into the ravines and pores of the lignin−nanoalloy structures quickly and came in contact with the catalyst frequently. Compared with the single-component Au NPs or Pd NPs, the electrons could transfer more easily from the negatively charged BH_4^- to the partial surface of the positively charged Au−Pd nanoalloys (based on the XPS analysis), which was regarded as the synergistic effect of Au and Pd.[34] Subsequently, the electrons were delivered to 4-NP and the latter was converted to 4-AP and left the surface due to the convection generated during stirring, enabling continuous catalysis. After several catalysis cycles, the surface of the catalytic stirring bar became rougher, but the ravines and pores were retained due to the three-dimensional framework of the coated lignin, where the Au−Pd nanoalloys were also protected by the stabilization effect of lignin, resulting in the preserved catalytic efficiency of the catalytic stirring bar over multiple cycles of reactions.

CONCLUSIONS

In summary, a novel and facile strategy was developed to fabricate the special magnetic catalyst, using Au−Pd nanoalloys as active ingredients, which were directly attached to the surface of a commercial magnetic stirring bar. The Au−Pd nanoalloys synthesized by lignin as the reducing and stabilizing agent exhibited a core−shell structure, with Au NPs as the core surrounded by the Pd shell. The prepared nanoalloys were coated onto the surface of a stirring bar with the aid of a commercial spray adhesive. The catalytic performance of the fabricated Au−Pd nanoalloys-coated catalytic stirring bar was validated by the reduction of 4-NP to 4-AP by $NaBH_4$, demonstrating an excellent catalytic activity compared with the single-component nanoparticles as catalysts. Our study not only proved the feasibility of biomass residuals lignin for the green synthesis of nanoalloys but also provided a novel and useful strategy for the fabrication of solid/liquid catalytic platforms. Although the magnetic stirring bar was used as a proof-of-concept example, we expect convenient extension of this approach to many other solid surfaces for future applications.

DOI: 10.1021/acsomega.7b00830
ACS Omega 2017, 2, 4938−4945

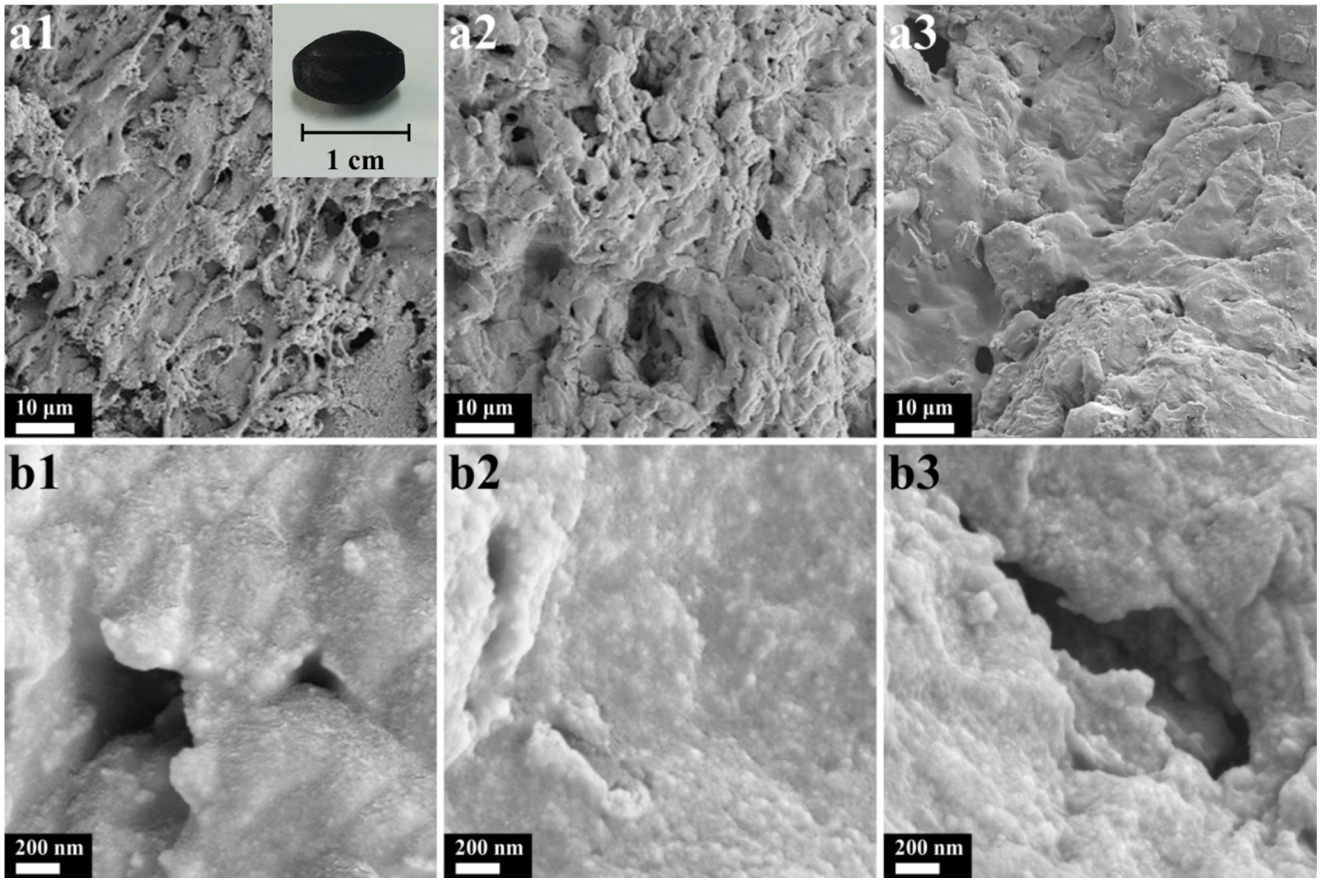

Figure 4. SEM images showing the surface of the Au−Pd nanoalloys-coated catalytic stirring bar at (a) lower magnification and (b) higher magnification: (1) uncatalyzed; (2) catalyzed for two cycles; and (3) catalyzed for seven cycles. The inset in (a1) shows the photograph of a fabricated Au−Pd nanoalloys-coated catalytic stirring bar. After catalysis, the rough surface of lignin−nanoalloy became smooth due to external swelled-up lignin (in lower magnification) and the surface of lignin−nanoalloy layer became rougher as more internal Au−Pd nanoalloys became exposed (in higher magnification).

Scheme 2. Proposed Mechanism of the Catalytic Reduction of 4-NP to 4-AP by $NaBH_4$ in the Presence of the Au−Pd Nanoalloys-Coated Catalytic Stirring Bar[a]

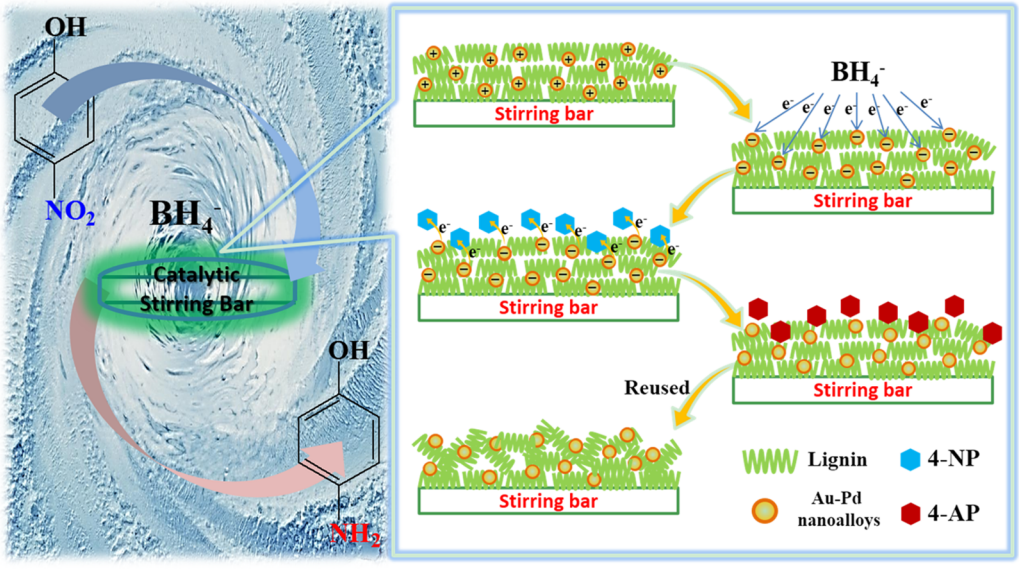

[a]Under stirring, 4-NP and BH_4^- came in contact with catalyst quickly. Electrons could transfer from BH_4^- to the positively charged Au−Pd nanoalloys and then 4-NP was reduced to 4-AP.

DOI: 10.1021/acsomega.7b00830
ACS Omega 2017, 2, 4938−4945

EXPERIMENTAL SECTION

Materials and Apparatus. Lignin was recovered from soda pulping effluent of the State Key Laboratory of Pulp and Paper Engineering (Guangzhou, China). Diammine dichloropalladium(II) ($Pd(NH_3)_2Cl_2$) and gold(III) chloride hydrate ($HAuCl_4{\cdot}xH_2O$) were supplied by Shanghai Macklin Biochemical Co., Ltd. (Shanghai, China). A Super 77 spray adhesive was obtained from 3M (Minneapolis). All of the other chemical reagents and solvents were of analytical grade.

An XH-100A microwave synthesis system was purchased from Beijing XiangHu Science and Technology Department Co., Ltd. (Beijing, China). The reaction was performed inside the system under pulsed microwave irradiation at atmospheric pressure.

Green Synthesis of Lignin−Au−Pd Composites. The synthesis of Au−Pd nanoalloys was conducted in lignin aqueous solution via a successive reduction process. Briefly, 2% lignin solution was prepared by dissolving lignin in 1% aqueous NaOH. Lignin solution was added in a certain volume of $HAuCl_4$ solution (40 mg/mL) at the solid mass ratio of 1:1, and the mixture was reacted under microwave irradiation (800 W, 80 °C) for 60 min for the formation of Au NPs. A certain amount of $Pd(NH_3)_2Cl_2$ was dissolved in 1% NaOH and then added into the above purple Au NPs solution, followed by the addition of extra 2% lignin solution (the mass ratio of Pd salt to lignin was 1:1) for the second step of reduction. After microwave irradiation for another 60 min at 90 °C, the resultant black solution was dialyzed against ultrapure water and the solid product was obtained after lyophilization at −40 °C. The products were denoted as $Au_{2.0}Pd_{1.0}$, $Au_{1.0}Pd_{1.0}$, and $Au_{0.5}Pd_{1.0}$, respectively, corresponding to the different feeding Au/Pd molar ratios. The single-component Au NPs or Pd NPs were also prepared as controls.

Fabrication of Au−Pd Nanoalloys-Coated Catalytic Magnetic Stirring Bar. For the facile fabrication of a novel catalytic magnetic stirring bar, a certain amount of Au−Pd nanoalloy a solid product was placed in a beaker onto an on-state magnetic stirring apparatus. A commercial magnetic stirring bar coated with fresh spray adhesive was place in the above container and stirred for a few seconds until agglutination. The stirring bar coated with Au−Pd nanoalloys was washed with ultrapure water for several times to remove the unbound solid and then dried in ambient conditions.

Characterization. The UV−vis spectra of the Au−Pd nanoalloys in different compositions were obtained by a UV-1800 spectrophotometer (Shimadzu, Japan), with a scan range of 300−900 nm at a scan interval of 0.5 nm. To investigate the crystal structure of Au−Pd nanoalloys, the X-ray diffractometer (XRD) analysis was performed on a D8 Advance XRD system (Cu Kα radiation, 40 kV, 50 mA) (Bruker, Germany) and the relative intensity was recorded in the scattering range (2θ) of 30−90°. The X-ray photoelectron spectroscopy (XPS) analysis of the Au−Pd nanoalloys was obtained by a Kratos AXIS Ultra DLD (Kratos, U.K.) using Mg Kα radiation ($h\gamma$ = 1253.6 eV) in step size of 0.1 eV, and the core-level data were analyzed with nonlinear fitting software (XPSPEAK 4.1). The structures of lignin before and after reduction were identified by the Fourier transform infrared (FT-IR) on a Nicolet 5700 spectrophotometer (Madison), using a spectral window of 4000−400 cm^{-1}.

The morphology and microstructures of the Au−Pd nanoalloys were observed by a JEM-2100F transmission electron microscope (TEM; JEOL, Japan) at an accelerating voltage of 200 kV. The scanning transmission electron microscopy−energy-dispersive X-ray spectrometry (STEM−EDS) maps of Pd and Au were conducted on a Bruker XFlash 5030T X-ray energy-dispersive spectroscopy analyzer (Bruker, Germany) attached to the equipment. A Zeiss Ultra 55 scanning electron microscope (SEM; Carl Zeiss, Germany) was employed at 5 kV to investigate the surface morphology of the prepared Au−Pd nanoalloys-coated catalytic magnetic stirring bar. The Au and Pd contents of the prepared catalysts were determined by Z-5000 atomic absorption spectrometer (AAS) (Hitachi, Japan).

Heterogeneous Catalytic Activity. The catalytic activity of the magnetic stirring bar was studied via a typical catalytic reaction, that is, the reduction of 4-NP to 4-AP in the presence of $NaBH_4$. The aqueous solution was prepared by mixing $NaBH_4$ (1 mL, 0.12 M) with 4-NP solution (0.5 mL, 0.005 M) and 25 mL of water. The olive-colored solution was placed onto a magnetic stirring apparatus, followed by the addition of the catalytic stirring bar. At required time intervals, the reaction solution was tested with the UV−vis spectrometer. The effect of different compositions of the Au/Pd coating on the catalytic magnetic stirring bar and stirring rate on the rate constant (k) were investigated. Furthermore, the recyclability and the change in the surface morphology of the stirring bar were also studied.

ASSOCIATED CONTENT

Supporting Information

The Supporting Information is available free of charge on the ACS Publications website at DOI: 10.1021/acsomega.7b00830.

FT-IR spectra; UV−vis spectra; size distribution (PDF)

AUTHOR INFORMATION

Corresponding Authors

*E-mail: xyw@scut.edu.cn (X.W.).

*E-mail: Zhang yszhang@research.bwh.harvard.edu (Y.S.Z.).

ORCID

Xiaoying Wang: 0000-0002-9303-6509

Yu Shrike Zhang: 0000-0001-8642-133X

Runcang Sun: 0000-0003-2721-6357

Author Contributions

§G.H. and X.L. contributed equally to this work.

Funding

This work was financially supported by the State Key Laboratory of Pulp and Paper Engineering, China (No. 2016TS02); the National Natural Science Foundation of China (Nos. 51403069 and 31622044); and Natural Science Foundation of Guangdong Province, China (No. 2014A030313252).

Notes

The authors declare no competing financial interest.

ACKNOWLEDGMENTS

G.H. and X.L. performed the experiment, analyzed the data, and wrote the manuscript; J.L. performed some experiments and revised the manuscript; X.W. and Y.S.Z. supervised the project and revised the manuscript; R.S. revised the manuscript.

REFERENCES

(1) Yang, F.; Wang, C.; Wang, L.; Liu, C.; Feng, A.; Liu, X.; Chi, C.; Jia, X.; Zhang, L.; Li, Y. Au/graphene oxide/carbon nanotube flexible

DOI: 10.1021/acsomega.7b00830
ACS Omega 2017, 2, 4938−4945

catalyst film: synthesis, characterization and its application for catalytic reduction of 4-nitrophenol. *RSC Adv.* **2015**, *5*, 37710−37715.
(2) Dong, Z.; Le, X.; Dong, C.; Zhang, W.; Li, X.; Ma, J. Ni@Pd core−shell nanoparticles modified fibrous silica nanospheres as highly efficient and recoverable catalyst for reduction of 4-nitrophenol and hydrodechlorination of 4-chlorophenol. *Appl. Catal., B* **2015**, *162*, 372−380.
(3) Hu, S.; Munoz, F.; Noborikawa, J.; Haan, J.; Scudiero, L.; Ha, S. Carbon supported Pd-based bimetallic and trimetallic catalyst for formic acid electrochemical oxidation. *Appl. Catal., B* **2016**, *180*, 758−765.
(4) Gu, W.; Deng, X.; Jia, X.; Li, J.; Wang, E. Functionalized graphene/Fe_3O_4 supported AuPt alloy as a magnetic, stable and recyclable catalyst for a catalytic reduction reaction. *J. Mater. Chem. A* **2015**, *3*, 8793−8799.
(5) Zhang, Z.; Zhou, Y.; Zhang, Y.; Zhou, S.; Xiang, S.; Sheng, X.; Jiang, P. A highly reactive and magnetic recyclable catalytic system based on AuPt nanoalloys supported on ellipsoidal Fe@SiO_2. *J. Mater. Chem. A* **2015**, *3*, 4642−4651.
(6) Villa, A.; Wang, D.; Su, D. S.; Prati, L. New challenges in gold catalysis: bimetallic systems. *Catal. Sci. Technol.* **2015**, *5*, 55−68.
(7) Guo, X.; Brault, P.; Zhi, G.; Caillard, A.; Guoqiang, J.; Coutanceau, C.; Baranton, S.; Guo, X. Synergistic Combination of Plasma Sputtered Pd-Au Bimetallic Nanoparticles for Catalytic Methane Combustion. *J. Phys. Chem. C* **2011**, *115*, 11240−11246.
(8) Ferrando, R.; Jellinek, J.; Johnston, R. L. Nanoalloys: from theory to applications of alloy clusters and nanoparticles. *Chem. Rev.* **2008**, *108*, 845−910.
(9) Lu, F.; Sun, D.; Huang, J.; Du, M.; Yang, F.; Chen, H.; Hong, Y.; Li, Q. Plant-mediated synthesis of Ag-Pd alloy nanoparticles and their application as catalyst toward selective hydrogenation. *ACS Sustainable Chem. Eng.* **2014**, *2*, 1212−1218.
(10) Kumari, M. M.; Jacob, J.; Philip, D. Green synthesis and applications of Au-Ag bimetallic nanoparticles. *Spectrochim. Acta, Part A* **2015**, *137*, 185−192.
(11) Shen, Z.; Luo, Y.; Wang, Q.; Wang, X.; Sun, R. High-value utilization of lignin to synthesize Ag nanoparticles with detection capacity for Hg^{2+}. *ACS Appl. Mater. Interfaces* **2014**, *6*, 16147−16155.
(12) Rhim, J.-W.; Kanmani, P. Synthesis and characterization of biopolymer agar mediated gold nanoparticles. *Mater. Lett.* **2015**, *141*, 114−117.
(13) Zhan, G.; Huang, J.; Du, M.; Abdul-Rauf, I.; Ma, Y.; Li, Q. Green synthesis of Au-Pd bimetallic nanoparticles: single-step bioreduction method with plant extract. *Mater. Lett.* **2011**, *65*, 2989−2991.
(14) Cortie, M. B.; McDonagh, A. M. Synthesis and optical properties of hybrid and alloy plasmonic nanoparticles. *Chem. Rev.* **2011**, *111*, 3713−3735.
(15) Feng, J.; Ma, C.; Miedziak, P. J.; Edwards, J. K.; Brett, G. L.; Li, D.; Du, Y.; Morgan, D. J.; Hutchings, G. J. Au-Pd nanoalloys supported on Mg-Al mixed metal oxides as a multifunctional catalyst for solvent-free oxidation of benzyl alcohol. *Dalton Trans.* **2013**, *42*, 14498−14508.
(16) Denton, A. R.; Ashcroft, N. W. Vegard's law. *Phys. Rev. A* **1991**, *43*, 3161.
(17) Xu, W.; Yi, H.; Yuan, Y.; Jing, P.; Chai, Y.; Yuan, R.; Wilson, G. S. An electrochemical aptasensor for thrombin using synergetic catalysis of enzyme and porous Au@Pd core-shell nanostructures for signal amplification. *Biosens. Bioelectron.* **2015**, *64*, 423−428.
(18) Yuan, X.; Sun, G.; Asakura, H.; Tanaka, T.; Chen, X.; Yuan, Y.; Laurenczy, G.; Kou, Y.; Dyson, P. J.; Yan, N. Development of palladium surface-enriched heteronuclear Au-Pd nanoparticle dehalogenation catalysts in an ionic liquid. *Chem. − Eur. J.* **2013**, *19*, 1227−1234.
(19) Xie, S.; Deng, J.; Zang, S.; Yang, H.; Guo, G.; Arandiyan, H.; Dai, H. Au-Pd/3DOM Co_3O_4: highly active and stable nanocatalysts for toluene oxidation. *J. Catal.* **2015**, *322*, 38−48.
(20) Zhang, K.; Yao, S.; Li, G.; Hu, Y. One-step sonoelectrochemical fabrication of gold nanoparticle/carbon nanosheet hybrids for efficient surface-enhanced Raman scattering. *Nanoscale* **2015**, *7*, 2659−2666.
(21) Casas, A.; Oliet, M.; Alonso, M.; Rodriguez, F. Dissolution of *Pinus radiata* and *Eucalyptus globulus* woods in ionic liquids under microwave radiation: lignin regeneration and characterization. *Sep. Purif. Technol.* **2012**, *97*, 115−122.
(22) Fernandes, D.; Hechenleitner, A. W.; Pineda, E. G. Kinetic study of the thermal decomposition of poly(vinyl alcohol)/kraft lignin derivative blends. *Thermochim. Acta* **2006**, *441*, 101−109.
(23) Hu, L.; Pan, H.; Zhou, Y.; Hse, C.-Y.; Liu, C.; Zhang, B.; Xu, B. Chemical groups and structural characterization of lignin via thiol-mediated demethylation. *J. Wood Chem. Technol.* **2014**, *34*, 122−134.
(24) Ferrando, R.; Jellinek, J.; Johnston, R. L. Nanoalloys: From Theory to Applications of Alloy Clusters and Nanoparticles. *Chem. Rev.* **2008**, *108*, 845−910.
(25) Chiou, J. R.; Lai, B. H.; Hsu, K. C.; Chen, D. H. One-pot green synthesis of silver/iron oxide composite nanoparticles for 4-nitrophenol reduction. *J. Hazard. Mater.* **2013**, *248−249*, 394−400.
(26) Li, X.; Liu, B.; Ye, W.; Wang, X.; Sun, R. Effect of rectorite on the synthesis of Ag NP and its catalytic activity. *Mater. Chem. Phys.* **2015**, *151*, 301−307.
(27) Ling, Y.; Zeng, X.; Tan, W.; Luo, J.; Liu, S. Quaternized chitosan/rectorite/AgNP nanocomposite catalyst for reduction of 4-nitrophenol. *J. Alloys Compd.* **2015**, *647*, 463−470.
(28) Li, J.; Zheng, Y.; Zeng, J.; Xia, Y. Controlling the size and morphology of Au@Pd core-shell nanocrystals by manipulating the kinetics of seeded growth. *Chem. − Eur. J.* **2012**, *18*, 8150−8156.
(29) Henning, A. M.; Watt, J.; Miedziak, P. J.; Cheong, S.; Santonastaso, M.; Song, M.; Takeda, Y.; Kirkland, A. I.; Taylor, S. H.; Tilley, R. D. Gold-palladium core-shell nanocrystals with size and shape control optimized for catalytic performance. *Angew. Chem.* **2013**, *125*, 1517−1520.
(30) Chen, Q.; Tanaka, S.; Fujita, T.; Chen, L.; Minato, T.; Ishikawa, Y.; Chen, M.; Asao, N.; Yamamoto, Y.; Jin, T. The synergistic effect of nanoporous AuPd alloy catalysts on highly chemoselective 1, 4-hydrosilylation of conjugated cyclic enones. *Chem. Commun.* **2014**, *50*, 3344−3346.
(31) Zeng, H.-y.; Feng, Z.; Deng, X.; Li, Y.-q. Activation of Mg-Al hydrotalcite catalysts for transesterification of rape oil. *Fuel* **2008**, *87*, 3071−3076.
(32) Huang, X.; Xiao, Y.; Zhang, W.; Lang, M. In-situ formation of silver nanoparticles stabilized by amphiphilic star-shaped copolymer and their catalytic application. *Appl. Surf. Sci.* **2012**, *258*, 2655−2660.
(33) Wunder, S.; Polzer, F.; Lu, Y.; Mei, Y.; Ballauff, M. Kinetic analysis of catalytic reduction of 4-nitrophenol by metallic nanoparticles immobilized in spherical polyelectrolyte brushes. *J. Phys. Chem. C* **2010**, *114*, 8814−8820.
(34) Nutt, M. O.; Hughes, J. B.; Wong, M. S. Designing Pd-on-Au bimetallic nanoparticle catalysts for trichloroethene hydrodechlorination. *Environ. Sci. Technol.* **2005**, *39*, 1346−1353.

DOI: 10.1021/acsomega.7b00830
ACS Omega 2017, 2, 4938−4945